PROCEEDINGS OF THE ROYAL SOCIETY A MATHEMATICAL, PHYSICAL & ENGINEERING SCIENCES

Pattern formation on the surface of a bubble driven by an acoustic field

A. O. Maksimov and T. G. Leighton

Proc. R. Soc. A 2012 **468**, 57-75 first published online 17 August 2011
doi: 10.1098/rspa.2011.0366

PROCEEDINGS OF THE ROYAL SOCIETY A

Proc. R. Soc. A (2012) **468**, 57–75
doi:10.1098/rspa.2011.0366
Published online 17 August 2011

Pattern formation on the surface of a bubble driven by an acoustic field

By A. O. Maksimov[1] and T. G. Leighton[2,*]

[1]*Pacific Oceanological Institute, Far Eastern Branch of the Russian Academy of Sciences, Vladivostok 690041, Russia*
[2]*Institute of Sound and Vibration Research, University of Southampton, Highfield, Southampton SO17 1BJ, UK*

The final stable shape taken by a fluid–fluid interface when it experiences a growing instability can be important in determining features as diverse as weather patterns in the atmosphere and oceans, the growth of cell structures and viruses, and the dynamics of planets and stars. An example which is accessible to laboratory study is that of an air bubble driven by ultrasound when it becomes shape-unstable through a parametric instability. Above the critical driving pressure threshold for shape oscillations, which is minimal at the resonance of the breathing mode, regular patterns of surface waves are observed on the bubble wall. The existing theoretical models, which take account only of the interaction between the breathing and distortion modes, cannot explain the selection of the regular pattern on the bubble wall. This paper proposes an explanation which is based on the consideration of a three-wave resonant interaction between the distortion modes. Using a Hamiltonian approach to nonlinear bubble oscillation, corrections to the dynamical equations governing the evolution of the amplitudes of interacting surface modes have been derived. Steady-state solutions of these equations describe the formation of a regular structure. Our predictions are confirmed by images of patterns observed on the bubble wall.

Keywords: bubble; Faraday ripples; symmetry breaking; pattern formation

1. Introduction

The shape taken by a fluid–fluid interface (liquid drops in liquids or gases, bubbles, interfaces between fluid layers) can influence a great many features in the modern world. On the microscopic scale, these include the growth of viruses and cell structures such as tumours (Chaplain *et al.* 2001), and the buckling of ultrasonic echocontrast agents (Sijl *et al.* 2011). On a larger scale, the chosen

*Author for correspondence (t.g.leighton@soton.ac.uk).

Electronic supplementary material is available at http://dx.doi.org/10.1098/rspa.2011.0366 or via http://rspa.royalsocietypublishing.org.

Received 8 June 2011
Accepted 18 July 2011

interface shape determines the production and motion of bubbles, droplets and aerosols (industrial, medicinal and in the ocean, where they affect global climate) and the formation of internal waves in the ocean and the atmosphere with their commensurate effects on the environment and life (Brooks *et al.* 2009). On a still larger scale, the growth of perturbations in the fluid shape of planetary gas giants and distant stars determines their evolution, and the final oscillatory shape can be used to interpret the forces at work (Brown & Kotak 1998; Reese *et al.* 2006). All such perturbations grow from instabilities, often exhibiting sudden growth after threshold conditions are exceeded, and have a tendency to chaotic behaviour. How this process results in the choice of a final stable shape is clearly key to the development and final form of a wide range of biologically important structures. This paper addresses how that choice of stable final form has been made. The predictions are tested against data obtained from air bubbles in water.

If a gas bubble of radius R_0 in a liquid of sound speed c is driven by an acoustic wave of low circular 'pump' frequency ω (such that $\omega R_0/c \ll 1$), then, at all amplitudes of that driving wave, the bubble undergoes spherically symmetric wall oscillation (i.e. a breathing mode pulsation). However, if the amplitude of the driving waves exceeds a well-defined threshold, then the nonlinear response of the gas bubble results in parametrically generated shape oscillations, superimposed upon the pulsation. This effect (the generation of surface waves under acceleration normal to a liquid–gas interface) was first characterized 180 years ago by Faraday (1831).

The surface mode parametrically excited will be the one whose own natural frequency ω_l (where l is the order of the distortion mode) is closest to the subharmonic of the pump frequency, i.e. the mode for which $\omega_l \approx \omega/2$. The driving acoustic pressure which excites a surface mode will have a minimum (the U-shaped threshold for the generation of surface waves) at a frequency close to the breathing mode resonance $\omega \approx \omega_0$ (where $\omega_0(R_0)$ is the natural frequency of the breathing mode).

The threshold conditions to excite a mode, and its form in steady state, have been discussed widely with studies (Longuet-Higgins 1989*a*,*b*, 1992; Mei & Zhou 1991; Asaki *et al.* 1993; Trinh *et al.* 1998) and reviews (Leighton 1994, 2004; Feng & Leal 1997) of the near-resonant interactions between breathing and distortion modes. To date, only selected applications have been realized for testing the theories in the laboratory, including bubble sizing (Leighton *et al.* 1996), the measurement of rectified diffusion (Birkin *et al.* 2004), cleaning (Birkin *et al.* 2011), the enhanced mixing in bioreactors or during electrodeposition (Leighton 2004; Offin *et al.* 2007) clearly attributed to microstreaming (Birkin *et al.* 2004; Leighton 2007*a*; Tho *et al.* 2007), and microbubble shape oscillations excited through ultrasonic parametric driving (Doinikov 2004; Dangla & Poulen 2010; Versluis *et al.* 2010; Prabowo & Ohl 2011). However, in between the well-established threshold condition and such studies of the effect of the shape chosen by the bubble in steady state, there is little work performed on the transient period between the two (Asaki & Marston 1997). In this regime, there exist significant differences in the times from inception taken to establish the steady-state pulsations and shape oscillations (Ramble *et al.* 1998). Near the threshold, one of the eigenvalues of the linear stability problem is small, causing the transient processes to be of very long duration (Maksimov & Leighton 2001). In particular,

the choice of which modes are chosen to grow to steady state, and which are selected out, determines from this potentially chaotic process the shape of the perturbation in steady state and hence the shape of a wide range of structures, having influences from the global to the cellular levels. Previous theories have covered the interaction between the breathing and distortion mode, but could not address the choice of the final shape. One study (Maksimov *et al.* 2008) considered interactions only between distortion modes (excluding the breathing mode), producing a method that was capable of predicting one final shape only in the form of wave packets consisting of many modes with different mode numbers l and localized as a result of self-focusing. This approach cannot be extended to predict the various final shapes that result from different insonification conditions, which requires a different physical basis, as provided by the method of this paper.

Experimental observations of patterns on the bubble wall have been reported in a number of publications (Hullin 1977; Trinh *et al.* 1998; Birkin *et al.* 2001, 2002; Watson *et al.* 2003; Leighton 2004; Dangla & Poulen 2010; Versluis *et al.* 2010), but elucidating the mechanisms for their realization is still an unsolved problem. Parametrical interaction between breathing and distortion modes cannot explain the selection in the growth of the initial distortions and the conditions for the realization of different final shapes. However, an approach for Faraday waves on a plane surface has been derived (Milner 1991; Miles 1993; Cross & Hohenberg 1993; Zhang & Vinals 1996). The key element for the formation of a regular pattern in the parametrically excited Faraday ripples is a three-wave resonant interaction between the ripples. The triad resonance appears to govern the selection of the roll, square or hexagon patterns formed by ripples. In this paper, we present a systematic account of this three-wave resonant interaction between the distortion modes. Minimization of the associated Lyapunov function allows prediction of the standing wave patterns for capillary waves.

2. Derivation of amplitude equations

To account for the three-wave resonant interaction of distortion modes, we use the Hamiltonian formulation of the nonlinear bubble dynamics (Maksimov 2008). The resulting canonical equations of motion are (Maksimov 2008)

$$\frac{\partial \xi}{\partial t} = \frac{\delta H}{\delta \Pi} \quad \text{and} \quad \frac{\partial \Pi}{\partial t} = -\frac{\delta H}{\delta \xi}, \tag{2.1}$$

where H is the Hamiltonian, and $\delta/\delta\xi$ and $\delta/\delta\Pi$ denote functional derivatives. We use the spherical coordinates (r, ϑ, α) with the equation of the bubble surface as $r = R_0 + \xi(\vartheta, \alpha, t)$, where R_0 is the equilibrium radius, ξ is the radial displacement, and α and ϑ are the azimuthal and polar angles. The Hamiltonian formulation assumes that the motion of the liquid near the bubble wall is irrotational and inviscid and can be described by the velocity potential φ. The boundary value of φ on the bubble wall is denoted by Φ. The variables $\Pi = -\rho_0(R_0 + \xi)^2\Phi(\vartheta, \alpha, t)$ and ξ are canonical (where ρ_0 is the equilibrium liquid density).

Unfortunately, H cannot be written in closed form as a functional of Π, ξ. However, one can limit the Hamiltonian to the first few terms of an expansion in powers of Π and ξ. The explicit form of the first two terms of $H \approx H_0 + H_1$ is given by equation (A 1) in appendix A.

Expansion of the variables in a series of spherical harmonics Y_{lm} can be considered as a canonical transformation

$$\left.\begin{aligned} \xi(\vartheta,\alpha,t) &= \sum_{l=0}^{\infty}\sum_{m=-l}^{l} \xi_{lm}(t)\, Y_{lm}(\vartheta,\alpha) \\ \text{and} \qquad \Pi(\vartheta,\alpha,t) &= \sum_{l=0}^{\infty}\sum_{m=-l}^{l} \Pi_{lm}(t)\, Y_{lm}(\vartheta,\alpha). \end{aligned}\right\} \tag{2.2}$$

The transformations of the monopole ($l=0$) and surface ($l\geq 2$) components can be used to diagonalize the quadratic Hamiltonian

$$\left.\begin{aligned} H_0 &= \omega_0 a_{00}^* a_{00} + \sum_{m=-1}^{1} \frac{\Pi_{1m}^* \Pi_{1m}}{\rho_0 R_0^3} + \sum_{l=2}^{\infty}\omega_l \sum_{m=-l}^{l} a_{lm}^* a_{lm}, \\ \Pi_{lm} &= -\frac{\mathtt{i}}{\sqrt{2}}\left(\frac{2\rho_0 R_0^3 \omega_l}{(l+1)}\right)^{1/2} (a_{lm} - (-1)^m a_{l-m}^*), \\ \xi_{lm} &= \frac{1}{\sqrt{2}}\left(\frac{\rho_0 R_0^3 \omega_l}{(l+1)}\right)^{-1/2} (a_{lm} + (-1)^m a_{l-m}^*) \\ \text{and} \qquad \Pi_{00} &= -\frac{\mathtt{i}}{\sqrt{2}}(2\rho_0 R_0^3 \omega_0)^{1/2}(a_{00} - a_{00}^*), \quad \xi_{00} = \frac{1}{\sqrt{2}}(\rho_0 R_0^3 \omega_0)^{-1/2}(a_{00} + a_{00}^*). \end{aligned}\right\} \tag{2.3}$$

The quadratic Hamiltonian demonstrates the existence of the following modes: the bulk modes ($l=0$ and $l=1$), i.e. the monopole pulsations ($l=0$) at the frequency $\omega_0 = \sqrt{3\gamma(P_\infty + 2\sigma/R_0)/(\rho_0 R_0^2)}$; the dipole modes ($l=1$) corresponding to the translational motions; and the shape oscillations ($l\geq 2$), which have the form of surface capillary waves propagating over the surface of the bubble at the frequency $\omega_l = \sqrt{\sigma(l+1)(l+2)(l-1)/(\rho_0 R_0^3)}$.

The appearance of surface modes ($l=2-16$) on inclusions of sizes ranging from several micrometres to several millimetres has been observed in recent years. The majority of the experiments have been performed with bubbles tethered to a wall, a wire, a fibre or a glass rod (Howkins 1965; Hullin 1977; Gorskii *et al.* 1988; Leighton *et al.* 1991, 1997; Phelps & Leighton 1996; Birkin *et al.* 2004; Bremond *et al.* 2005*a*). The dynamics of a tethered bubble differ from the behaviour of a free bubble (Blue 1967; Leighton 1994; Weninger *et al.* 1997; Bremond *et al.* 2005*b*; Maksimov 2005). Since the experimental observations reported here did

not include significant translational motion (this will not necessarily be true for all tethered bubbles (Tho *et al.* 2007; Birkin *et al.* in press)), if the contact area is small compared with the total area of the bubble, the observed effect of tethering can be relatively weak. The presence of a contact leads to the suppression of translational motions, namely the dipole mode. Hence, the experimental results can be interpreted with allowance made only for the monopole and surface distortions in the Hamiltonian description.

The canonical equations in amplitude variables take the form:

$$\frac{\mathrm{d}a_{lm}}{\mathrm{d}t} = -\mathtt{i}\frac{\partial H}{\partial a^*_{lm}}. \tag{2.4}$$

The parametric generation of the Faraday ripples is a consequence of the contribution of the third-order nonlinear terms H_{mss} in the expansion of the Hamiltonian, describing the interaction between the breathing (monopole) mode and the two distortion (surface) modes (Maksimov (2008); see equation (A 2) for details of the structure of H_{mss}). The experimental conditions studied to date have examined the following two near-resonant interactions: $\omega \approx \omega_0$ and $\omega_0 \approx 2\omega_l$.

To account for the three-wave resonant interaction between the ripples, we should consider the third-order nonlinear terms in the Hamiltonian which describe the interaction between the three distortion modes H_{sss} (Maksimov (2008); the explicit form of H_{sss} is given by equation (A 3)). By using the explicit form of the Hamiltonian (A 2 and A 3), we can find the structure of the canonical equations of motion (2.4) for amplitudes of the monopole mode a_{00}, the parametrically unstable distortion mode a_{lm} and the partner of the resonant triad $a_{n'm'}$. The resonant triad is formed by two unstable waves with the same frequencies ω_l interacting to form a wave of higher frequency $\omega_{n'} \approx 2\omega_l$. These equations are obtained by differentiation of the Hamiltonian with respect to a^*_{00}, a^*_{lm}, $a^*_{n'm'}$ and retaining only the resonant terms having the same time evolution as a_{00}, a_{lm}, $a_{n'm'}$.

In such circumstances, the slowly varying complex amplitudes of the breathing $\hat{a}_{00} = a_{00}\exp(\mathtt{i}\omega t)$ and distortion modes $\hat{a}_{lm} = a_{lm}\exp(\mathtt{i}(\omega/2)t)$, $\hat{a}_{n'm'} = a_{n'm'}\exp(\mathtt{i}\omega t)$ satisfy the equations similar to ones derived by Maksimov & Leighton (2001), which have the form

$$\begin{aligned}\frac{\mathrm{d}\hat{a}_{00}}{\mathrm{d}t} &= [\mathtt{i}(\omega-\omega_0)-\gamma_0]\hat{a}_{00} - \mathtt{i}C_{ll0}\sum_{m=-l}^{l}(-1)^m\hat{a}_{lm}\hat{a}_{l-m} \\ &\quad + \frac{\sqrt{\pi}R_0^2P_m}{(2\rho_0R_0^3\omega_0)^{1/2}}, \qquad (2.5)\\ \frac{\mathrm{d}\hat{a}_{lm}}{\mathrm{d}t} &= \left[\mathtt{i}\left(\frac{\omega}{2}-\omega_l\right)-\gamma_l\right]\hat{a}_{lm} - 2\mathtt{i}C_{ll0}(-1)^m\hat{a}_{00}\hat{a}^*_{l-m} \\ &\quad + 2\mathtt{i}C_{n'll}\sum_{n'}\sum_{m'=-n'}^{n'}(-1)^{m'}\overline{Y_{n'm'}Y_{l-m}Y_{lm-m'}}\hat{a}_{n'm'}\hat{a}^*_{lm-m'} \qquad (2.6)\end{aligned}$$

and
$$\frac{\mathrm{d}\hat{a}_{n'm'}}{\mathrm{d}t} = [\mathtt{i}(\omega - \omega_{n'}) - \gamma_{n'}]\hat{a}_{n'm'} + 2\mathtt{i}\, C_{n'll} \sum_{m_1=-l}^{l} (-1)^{m_1} \overline{Y_{n'-m'}\, Y_{lm_1}\, Y_{lm'-m_1}}\, \hat{a}_{lm_1}\, \hat{a}_{ln'-m_1}, \tag{2.7}$$

where $C_{ll0} = (2^7\pi)^{-1/2}(4l-1)\omega_l(\rho_0 R_0^3\omega_0)^{-1/2}R_0^{-1}$ is the coupling coefficient in the energy of interaction of the breathing and distortion modes. The coupling coefficient in the energy of interaction of the distortion modes $C_{n'll}$ has the form

$$C_{n'll} = \frac{\omega_l}{(2^5\rho_0 R_0^5\omega_{n'})^{1/2}} \left\{ \frac{(n'+1)^{1/2}}{(l+1)} \left[\frac{n'(n'+1)}{2} - 3(l+1) + \frac{2}{3}\frac{(l+1)}{(l+2)(l-1)} \right] + \frac{\omega_{n'}}{\omega_l(n'+1)^{1/2}} \left[n'(n'+1) - 2(n'+1)(l-1) + 4(l+1) + \frac{(n'+1)(l+1)\omega_2^2}{9\omega_{n'}\omega_l} \right] \right\}.$$

Note that the canonical transformation (2.3) leads to a different normalization factor in the definition of the amplitude a_{lm} from those used by Maksimov & Leighton (2001).

The damping of the breathing mode γ_0 and the distortion modes of order l and n' (i.e. γ_l and $\gamma_{n'}$) are included in the current model. We have so far assumed the flow near the bubble to be inviscid and irrotational. In reality, the presence of viscosity implies that at the surface of the bubble the two tangential components of the stress must be continuous, while the normal component (which includes a viscous term) has a given discontinuity owing to surface tension. To accommodate these boundary conditions, solutions of the viscous equations of motion are required. The introduction of viscous terms into the equation of motion is characterized by a fundamental length $\delta = (2\nu/\omega)^{1/2}$ (where ν is the kinematic viscosity), a scale which has proved useful in describing both shape and breathing modes on bubble walls (Ainslie & Leighton in press). The viscous dissipation in the fluid surrounding the bubble may be calculated as though the flow were irrotational but only if the Stokes layers are relatively thin in comparison with the wavelength of the distortion mode (Longuet-Higgins 1989*b*). The damping factor evaluated by Longuet-Higgins (1989*b*) for this case leads to the formula given by Lamb: $\gamma_l = (l+2)(2l+1)\nu/R_0^2$. The damping factor for the breathing mode $\gamma_0 \approx \omega^2 R_0/2c + (2\nu/R_0^2) + 3(\gamma-1)(\omega_0/2R_0)(D/2\omega)^{1/2}$ is the sum of radiation damping, viscous damping and damping owing to thermal diffusion, as estimated by a linear analysis, where D is the diffusivity coefficient.

The correction terms which describe the interaction of the three modes are those which are proportional to $\hat{a}_{n'm'}\hat{a}^*_{lm-m'}$ in equation (2.6) and which, in equation (2.7), describe the evolution of the amplitude of the high-frequency

partner of the resonant triad. Some couplings, such as that between the breathing and n' modes, would require a fourth-order Hamiltonian H_2: currently, the algebraic sum of the natural frequencies $(2\omega_{n'} - \omega_0) \approx \omega_0$ $(\omega_{n'} \approx \omega_0)$ cannot vanish for such interactions $n' + n' \longleftrightarrow 0$, $n' + 0 \longleftrightarrow n'$, and so no resonant synchronization is possible. For this reason, we neglect the correction terms $\hat{a}_{n'm'}\hat{a}_{n'-m'}$ in equation (2.5) and $\hat{a}_{00}\hat{a}_{n'm'}$ in equation (2.7).

The occurrence of the three-wave resonance $\omega_{l_1} + \omega_{l_2} \approx \omega_{l_3}$ has been analysed by Maksimov (2008) numerically for each value of l_3 from 3 to 15. The resonance condition for the processes considered there is simpler and can be easily realized for $l \gg 1$, to give $n' \approx 4^{1/3} l$. The relative detuning for the resonant triads $|2\omega_l - \omega_{n'}|/\omega_l$ can be very small. For simplicity, we shall account for only one triad, specifically the one which is nearest to the resonance condition. An important peculiarity of the three-wave resonance is the restriction imposed by the law of conservation of parity: the sum of the mode numbers $2l + n'$ should be an even number.

3. Analysis of amplitude equations

The system of equations (2.5–2.7) can be significantly simplified using the master–slave principle known in applied mathematics as centre-manifold reduction (Wiggins 1996). The actual parametric instability occurs when one of the eigenvalues of the linear stability analysis (Maksimov & Leighton 2001)

$$\lambda_{1,2} = -\gamma_l \pm \left\{ \frac{P_m^2 (4l-1)^2}{16^2 \rho_0^2 R_0^4 \Delta_0} - \left(\omega_l - \frac{\omega}{2}\right)^2 \right\}^{1/2} \tag{3.1}$$

passes through zero at

$$\left.\begin{aligned} P_m^2 &= \left[\frac{16\rho_0 R_0^2}{(4l-1)}\right]^2 \Delta_0 \Delta_l, \\ \Delta_0 &= [(\omega_0 - \omega)^2 + \gamma_0^2], \quad \Delta_l = \left[\left(\omega_l - \frac{\omega}{2}\right)^2 + \gamma_l^2\right]. \end{aligned}\right\} \tag{3.2}$$

If the conditions are sufficiently close to the threshold of this instability, then we can further reduce the description by eliminating 'fast' variables (Cross & Hohenberg 1993; Maksimov & Leighton 2001). The breathing mode and the high-frequency (stable) distortion mode n' are fast-phased to draw energy from the pumping and unstable modes l. The linear combination of $\hat{a}_{lm}$ and $\hat{a}^*_{l-m}$ corresponding to the eigenvalue λ_2 is also fast. Thus, near the threshold, it is possible to rewrite equations (2.5)–(2.7) in terms of the slowly varying standing-wave amplitude B_{lm}

$$\left.\begin{aligned} B_{lm} &= \frac{1}{2\mathrm{i}}[\hat{a}_{lm}\, \mathrm{e}^{\mathrm{i}(\phi_2 - \phi_1)} - (-1)^m \hat{a}^*_{l-m}\, \mathrm{e}^{-\mathrm{i}(\phi_2 - \phi_1)}], \\ \sin\phi_1 &= \left(\omega_l - \frac{\omega}{2}\right)\Delta_l^{-1/2} \quad \text{and} \quad \sin\phi_2 = -\gamma_0 \Delta_0^{-1/2}. \end{aligned}\right\} \tag{3.3}$$

This yields

$$\left.\begin{aligned}
\frac{\mathrm{d}B_{lm}}{\mathrm{d}t} &= \lambda_1 B_{lm} - \frac{\partial}{\partial B^*_{lm}}[\Gamma_0 I_0^4(l) + \Gamma_{n'} I_{n'}^4(l)],\\
I_k^4(l) &= \frac{1}{4}\sum_{m'=-k}^{k}\sum_{m''=-k}^{k}\sum_{m_1=-l}^{l}\sum_{m_2=-l}^{l}\sum_{s_1=-l}^{l}\sum_{s_2=-l}^{l}\begin{pmatrix} k & k & 0\\ m' & m'' & 0\end{pmatrix}\\
&\quad\times\begin{pmatrix} l & l & k\\ m_1 & m_2 & -m'\end{pmatrix}\begin{pmatrix} l & l & k\\ s_1 & s_2 & -m''\end{pmatrix} B_{lm_1}B_{lm_2}B_{ls_1}B_{ls_2},\\
\Gamma_0 &= (C_{ll0})^2\left[\gamma_0\gamma_l - (\omega_0-\omega)\left(\omega_l - \frac{\omega}{2}\right)\right]\Delta_l\gamma_l^{-3}\Delta_0^{-1}\\
\text{and}\qquad \Gamma_{n'} &= 2(C_{n'll})^2\left[\gamma_{n'}\gamma_l - (\omega_{n'}-\omega)\left(\omega_l - \frac{\omega}{2}\right)\right]\Delta_l\\
&\quad\times\gamma_l^{-3}\Delta_{n'}^{-1}\begin{pmatrix} l & l & n'\\ 0 & 0 & 0\end{pmatrix}^2(2l+1)^2(2n'+1)(4\pi)^{-1}.
\end{aligned}\right\}\qquad(3.4)$$

Equation (3.4) is of gradient form

$$\frac{\partial B_{lm}}{\partial t} = -\frac{\partial F}{\partial B^*_{lm}},\quad \text{where}\quad F = -\lambda_1 I_0^2(l) + \Gamma_0 I_0^4(l) + \Gamma_{n'} I_{n'}^4(l),\qquad(3.5)$$

and thus is covariant (i.e. it has the same structure/form in different coordinate systems). The possibility of representing the m-linear covariant as the gradient of a $(m+1)$-linear invariant is restricted to $m \le 3$ (Gaeta 1985). This complicates the analysis for the case when the resonant triads are not effective and one should then account for the next approximation. Note that, in the current form, the theory cannot describe the patterns for the first mode numbers, as resonant interaction for these modes is not effective and it is necessary to account for higher nonlinear terms (corresponding to accounting for the fourth-order Hamiltonian H_2; Maksimov (2008)). The symmetry of the preferred pattern is that for which the Lyapunov functional F is lowest (Cross & Hohenberg 1993).

A number of far-from-equilibrium systems exhibit instabilities leading to the formation of spatial patterns. A basic feature of the non-equilibrium phase transition is the spontaneous breakdown of symmetry: as the control parameter is changed, the stable steady state of the system, which is invariant under a symmetry group $\mathbf{G}$, loses its stability and a new steady state appears which is invariant only under a subgroup of $\mathbf{G}$ (Rácz & Tél 1982). The set of B_{lm} forms the multi-component order parameter for the transition corresponding to the broken spherical symmetry. The number of components of the order parameter $2l+1$ is given by the dimension of the irreducible representation of the symmetry group.

What does it mean for a system (3.4) to be symmetrical under a group action? The group element $\gamma \in \mathbf{G}$ is a symmetry of a system written in the form of $\dot{\boldsymbol{x}} = \boldsymbol{f}(\boldsymbol{x})$ if, for every solution $\boldsymbol{x}(t) = (B_{lm_i})$, $\gamma\boldsymbol{x}(t)$ is also a solution. A condition for γ to be a symmetry is $\boldsymbol{f}(\gamma\boldsymbol{x}) = \gamma\boldsymbol{f}(\boldsymbol{x})$. If this holds, one says that $\boldsymbol{f}$ is γ-equivariant (Golubitsky *et al.* 1988). Thus, an important property of system (3.4) is that it is equivariant under the action of the original symmetry group of the

sphere $\mathbf{O}(3)$. ($\mathbf{O}(n)$ notation is used for the orthogonal group of degree n; $\mathbf{O}(3)$ is the group of 3×3 orthogonal matrices with the group operation of matrix multiplication.)

4. Solutions

The next task is to formulate the notation of the symmetry of a solution to an equivariant equation (3.4). Equilibria of equation (3.4) are the solutions of $\boldsymbol{f}(\boldsymbol{x}) = 0$. We can express the symmetries of the solution of the system (as opposed to the symmetry of the system) as follows (Golubitsky *et al.* 1988): a symmetry h of $\boldsymbol{x}$ is an element of $\mathbf{G}$ that leaves $\boldsymbol{x}$ invariant. The set of all such h is a subgroup of $\mathbf{G}$, known as the 'isotropy subgroup'. The isotropy subgroup of a solution of an equivariant system of ordinary differential equations provides useful information about the form of that solution.

Apart from the trivial solution of $B_{lm} = 0$ for $m = 0, 1, 2, \ldots l$ (note that according to the adopted normalization (3.3) $B_{l-m} = (-1)^m B^*_{lm}$), there is a family of solutions differing in the total number of standing waves N for which $B_{lm} \neq 0$. The search for stationary solutions to the $2l + 1$ equations (3.4) is significantly simplified by restricting the consideration to solutions with a particular symmetry corresponding to subgroups of the original symmetry group of the sphere $\mathbf{O}(3)$. These subgroups include $\mathbf{O}(2)$, $\mathbb{I}$ (icosahedron), $\mathbf{O}$ (cube), $\mathbf{T}$ (tetrahedron), $\mathbf{D}_n$ (regular n-gon) and $\mathbf{C}_n$ (directed n-gon). We use traditional (Scheonflies) notations (e.g. Landau & Lifshitz 1977). Note that the rolls, squares and hexagons observed on the plane surface correspond to subgroups of the circle $\mathbf{O}(2)$. We consider here the simplest cases ($N = 1, 2$), and full consideration based on analysis of all point groups (Golubitsky *et al.* 1988) will be the subject of future research.

For $N = 1$, there is only one standing wave B_{lm} and the steady-state solution of (4.3) has the form

$$\left.\begin{aligned} B^*_{lm} B_{lm} &= \left(\frac{\lambda_1}{\Gamma_0}\right)\left[(2 - \delta_{m,0}) + \left(\frac{\Gamma_{n'}}{\Gamma_0}\right) g(m)\right]^{-1}, \\ g(m) &= 2\begin{pmatrix} l & l & n' \\ -m & m & 0 \end{pmatrix}^2 + \begin{pmatrix} l & l & n' \\ -m & -m & 2m \end{pmatrix}^2 \Theta(n' - 2m), \quad m \neq 0 \\ \text{and} \qquad g(0) &= \begin{pmatrix} l & l & n' \\ 0 & 0 & 0 \end{pmatrix}^2, \quad m = 0, \end{aligned}\right\} \tag{4.1}$$

where Θ is the Heaviside step function. Evaluation of the Lyapunov function $F(m)$ at the local minima corresponding to the steady-state solutions (4.1) gives

$$F(m) = -\frac{\lambda_1^2}{2\Gamma_0}\left[(2 - \delta_{m,0}) + \left(\frac{\Gamma_{n'}}{\Gamma_0}\right) g(m)\right]^{-1}. \tag{4.2}$$

Direct calculations of the Wigner 3j symbols for mode numbers $l \geq 9$ corresponding to the domain of applicability of equation (3.4) shows that $g(l)$ is negligibly small in comparison with the other coefficients $g(m)$, indicating that

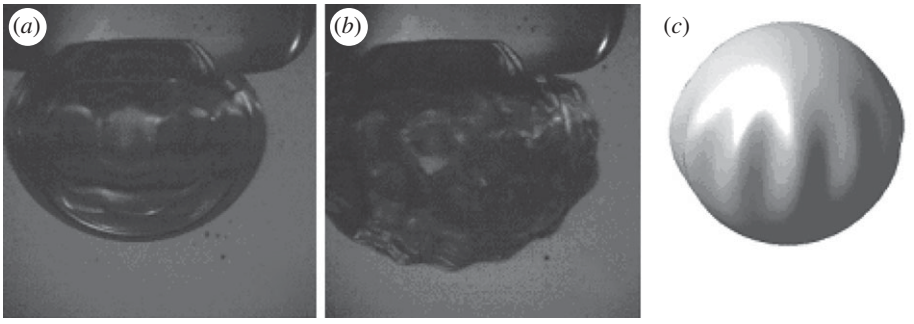

Figure 1. The images show a bubble as the amplitude of excitation increases: (*a*) 24 Pa, (*b*) 44 Pa (zero-to-peak). The mean radius of the bubble is approximately 2.1 mm and the driving field has frequency of 1.500 kHz. (*c*) The shape of rolls which are described by equation (4.8) with the same input data as conditions for the image shown in (*a*). The glass rod visible above the bubble in (*a*,*b*) prevents its buoyant rise (Birkin *et al.* 2002) (see also video at http://www.isvr.soton.ac.uk/fdag/Faraday.htm). Its effect is not included in the analysis. Photographs taken by Birkin & Watson.

the deepest minimum of the Lyapunov function is achieved at $m = l$. This is consistent with the physical idea that the triad-interaction should be least for the realized structure. Thus, we have

$$B_{ll}^{*} B_{ll} = \frac{\lambda_1}{2\Gamma_0}. \tag{4.3}$$

The pattern on the bubble wall is described by

$$r = R_0 + \xi_{00} Y_{00} + \sum_{m=-l}^{l} \xi_{lm} Y_{lm} + \sum_{m'=-n'}^{n'} \xi_{n'm'} Y_{n'm'} \approx R_0 + \left(\frac{l+1}{2\rho_0 R_0^3 \omega_l}\right)^{1/2} \times \left(\frac{\lambda}{2\Gamma_0}\right)^{1/2} \sqrt{\frac{2l+1}{4\pi} \frac{(2l)!}{2^{2l-4}(l!)^2}} \frac{\sin^l \vartheta \cos(l\alpha + \beta_l)}{\cos 2\phi_1} \times \sin\left[\left(\frac{\omega}{2}\right) t + (\phi_1 + \phi_2)\right], \tag{4.4}$$

where β_l is the phase of B_{ll}. The spherical harmonic corresponding to this state $Y_{ll} \sim \sin^l \vartheta$ has no oscillations along the meridian. The pattern corresponding to this solution is shown in figure 1*c* and can be named by analogy with structures observed on a plane surface: rolls. The steady-state amplitude of the n' mode is small as it is proportional to λ and the negligibly small factor $\sqrt{g(l)}$. The smallness of the radial amplitude in comparison with the amplitude of the distortion mode is discussed in detail by Maksimov & Leighton (2001). The isotropy group of this solution is $\mathbf{D}_{lh}$ of order $4l$: prismatic symmetry. It has l-fold rotational symmetry, the twofold rotation axes being perpendicular to the primary rotation axis and the horizontal reflection plane.

For patterns formed by two standing waves $N=2$, we have

$$B^*_{lm_1}B_{lm_1}=\left(\frac{\lambda_1}{\Gamma_0}\right)[g(m_1,m_2)-g(m_2)]\times\left\{(2-\delta_{m_2,0})[g(m_2,m_1)-g(m_1)]+(2-\delta_{m_1,0})[g(m_1,m_2)-g(m_2)]+\left(\frac{\Gamma_{n'}}{\Gamma_0}\right)[g(m_1,m_2)g(m_2,m_1)-g(m_1)g(m_2)]\right\}^{-1}. \tag{4.5}$$

The square of the amplitude of the second standing wave $B^*_{lm_2}B_{lm_2}$ is obtained from equation (4.5) by permutation of indexes m_1 and m_2. The coupling coefficients are symmetrical $g(m_1,m_2)=g(m_2,m_1)$. As the system tries to avoid the modes that participate in a triad-resonant interaction, it is reasonable to assume that one of the partners in the formation of these structures will be the mode $m_1=l$, as its self-interaction is negligibly small. Thus, letting $g(l)=0$ in the evaluation of the Lyapunov function, we have

$$\left.\begin{aligned}F(l,m_2)&=-\frac{\lambda_1}{2\Gamma_0}[g(m_2)-2g(l,m_2)]\times\left\{(2-\delta_{m_2,0})g(m_2)-(4-\delta_{m_2,0})g(l,m_2)-\left(\frac{\Gamma_{n'}}{\Gamma_0}\right)g(l,m_2)^2\right\}^{-1},\\ g(l,0)&=\begin{pmatrix}l&l&n'\\0&0&0\end{pmatrix}\begin{pmatrix}l&l&n'\\-l&l&0\end{pmatrix}+2\begin{pmatrix}l&l&n'\\-l&0&l\end{pmatrix}^2\\ \text{and}\quad g(l,m_2)&=2\begin{pmatrix}l&l&n'\\-l&m_2&l-m_2\end{pmatrix}^2+2\begin{pmatrix}l&l&n'\\-m_2&m_2&0\end{pmatrix}\begin{pmatrix}l&l&n'\\-l&l&0\end{pmatrix}\\ &\quad+\Theta(n'-2m_2)\begin{pmatrix}l&l&n'\\-l&-m_2&l+m_2\end{pmatrix}^2.\end{aligned}\right\} \tag{4.6}$$

The positive nature of B^*B imposes restrictions on the possible partners: mode numbers m_2, as the denominator of equation (4.5), and $[g(m_2)-2g(l,m_2)]$ should be negative. Thus, only $m_2\ll l$ can form this type of pattern. The final step requires numerical evaluation of the Wigner 3j symbols and we do this for the particular case corresponding to the specific pattern observed by Watson *et al.* (2003) and shown in figure 2*a*.

For an $l=15$ mode unstable on the wall of the bubble (of radius approx. 2.5 mm) which was driven at 1.297 kHz, with 83.5 Pa acoustic pressure, the most effective resonant triad is formed with the $n'=24$ mode. For these modes, the pre-factor entering into the ratio Γ_{24}/Γ_0 which does not depend on the driving frequency ω has been calculated for the following values of the determining parameters: $\gamma=1.4$ (polytropic exponent: air), $\sigma=7.2\times10^{-2}$ Nm (surface tension: clean water–air, 20°C), $P_0=10^5$ Pa (ambient pressure),

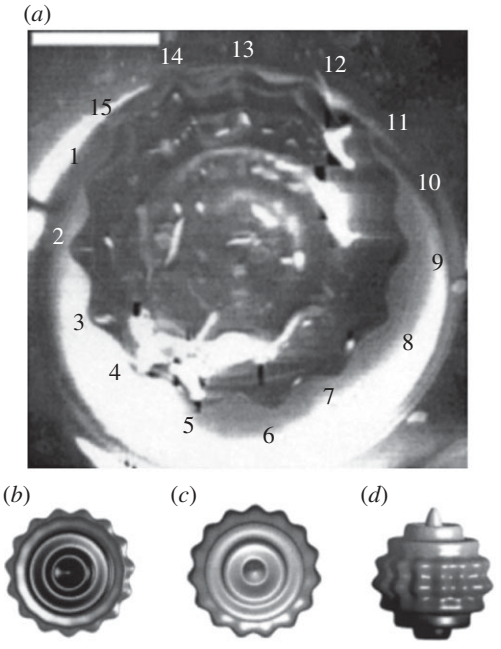

Figure 2. (*a*) View from below an air bubble, restrained against buoyant rise by a glass rod, visible as the white circle 'behind' the bubble. The bubble (of radius approx. 2.5 mm) was driven at 1.297 kHz, with 83.5 Pa zero-to-peak acoustic pressure amplitude. The bubble shape corresponding to a square pattern for these experimental conditions is shown in two-dimensional projections: (*b*) a view from below, (*c*) a top view, and (*d*) a side view. The photographic image in (*a*) is from Birkin *et al.* (2001) and Watson *et al.* (2003). (*a*) Scale bar, 2 mm.

$\rho_0 = 988\,\mathrm{kg\,m^{-3}}$ (equilibrium density liquid: water), $c = 1484\,\mathrm{m\,s^{-1}}$ (speed of sound in the liquid: water), $\nu = 10^{-6}\,\mathrm{m^2\,s^{-1}}$ (kinematic viscosity liquid: water), $D = 2 \times 10^{-5}\,\mathrm{m^2\,s^{-1}}$ (diffusion coefficient). The result is

$$\frac{\Gamma_{24}}{\Gamma_0} \approx 21 \frac{\gamma_{24}\gamma_{15} - (\omega - \omega_{24})(\omega/2 - \omega_{15})}{\gamma_0\gamma_{15} - (\omega - \omega_0)(\omega/2 - \omega_{15})}. \tag{4.7}$$

This allows evaluation of the governing parameter Γ_{24}/Γ_0 along the threshold curve and comparison of conditions for the realization of different patterns.

Calculations of $g(m_2)$ and $g(15, m_2)$ have been performed for $0 \le m_2 \le 15$. Substitution of these coefficients into equation (4.9) and evaluation of the Lyapunov function $F(15, m_2)$ demonstrate that it has a minimum value for $m_2 = 0$. In this case, the squared amplitudes (4.5) have the form

$$\left.\begin{aligned} B^*_{15\,15} B_{15\,15} &= \frac{\lambda_1}{\Gamma_0} \frac{g(15,0) - g(0)}{3g(15,0) - 2g(0) + (\Gamma_{24}/\Gamma_0) g(15,0)^2} \\ \text{and} \qquad B^*_{15\,0} B_{15\,0} &= \frac{\lambda_1}{\Gamma_0} \frac{g(15,0)}{3g(15,0) - 2g(0) + (\Gamma_{24}/\Gamma_0) g(15,0)^2}. \end{aligned}\right\} \tag{4.8}$$

Numerical evaluation of the Wigner 3j symbols gives

$$\left.\begin{aligned} B^*_{15\,15}B_{15\,15} &= \frac{\lambda_1}{2\Gamma_0}\frac{1}{1.855+(\Gamma_{24}/\Gamma_0)\,0.00558} \\ \text{and}\qquad B^*_{15\,0}B_{15\,0} &= \frac{\lambda_1}{2\Gamma_0}\frac{1}{1.082+(\Gamma_{24}/\Gamma_0)\,0.00334}. \end{aligned}\right\} \tag{4.9}$$

The pattern on the bubble wall is described by

$$r = R_0 + \left(\frac{1}{\rho_0 R_0^3\omega_{15}}\right)^{1/2}\left(\frac{\lambda}{2\Gamma_0}\right)^{1/2}\frac{2.4\sin[(\omega/2)t+(\phi_1+\phi_2)]}{\cos 2\phi_1} \times\left\{\frac{\sin^{15}\vartheta\cos(15\alpha+\beta_{15})}{[1.855+(\Gamma_{24}/\Gamma_0)0.00558]^{1/2}}+1.85\frac{P_{15}(\cos\vartheta)}{[1.082+(\Gamma_{24}/\Gamma_0)0.00334]^{1/2}}\right\}. \tag{4.10}$$

By analogy with the structures formed by orthogonal standing waves on a plane surface, it is reasonable to name this type of pattern as 'squares'. Figure 2 illustrates the shape of this 'square' pattern calculated on the basis of equation (4.10). The presence of the Legendre polynomial P_{15} (which is antisymmetric relative to reflection in the horizontal plane for odd l) changes the symmetry of this pattern in comparison with that of the 'rolls'. The isotropy group of this solution is $\mathbf{C}_{15v}$ of order 30, which has pyramidal symmetry: it has 15-fold rotational symmetry and a set of 15 mirror planes containing the axis.

5. Discussion

In order to validate the predications of this work, the experimental observations of patterns on the bubble wall have been processed. Figure 1*a*,*b* shows the patterns observed on the bubble wall when the driving pressure increased slightly from the near threshold value. The pattern corresponding to figure 1*a* is frequently observed in experiments (Birkin *et al.* 2002; Dangla & Poulain 2010). Transition to the polyhedral symmetry structure demonstrated by figure 2*b* corresponds to the case when insonification conditions differ significantly from those at threshold (the driving pressure is much greater than the threshold one, or the frequency differs significantly from that at threshold for this mode) and cannot be analysed with a simplified model equation (3.4). Nevertheless, it can be shown that any steady-state solution of equation (3.4) is a steady-state solution of equations (2.5)–(2.7). Far from the threshold, the amplitude equations (2.5)–(2.7) have no gradient form and the Lyapunov function cannot be determined, while the classification of solutions on the basis of point groups symmetry can be applied for all these states.

Of particular interest are patterns with the symmetry groups of the Platonic solids: the tetrahedron, the cube (or octahedron) containing **T** and the icosahedron (or dodecahedron) also containing **T**. An important relation between subgroups is that of containment (Golubitsky *et al.* 1988)—whether or not one subgroup is contained in another. Undertaking such an examination over the subgroups, one can define a partial ordering on the set. It classifies the possible ways for equilibrium to break the symmetry, and arranges them in a hierarchy

with the property that smaller isotropy subgroups tend to break more symmetries and thus are less probable. The icosahedral and cubic subgroups are maximal ones (a subgroup $\mathbf{H} \leq \mathbf{G}$ is called maximal if $\mathbf{H} \neq \mathbf{G}$ and the only subgroups of $\mathbf{G}$ which contain $\mathbf{H}$ are $\mathbf{H}$ and $\mathbf{G}$), but their realization depends on the degree of the spherical harmonic (the mode number). For the range of interest, $\mathbb{I}$ can be realized for $l = 8, 10, 12, 15$ (Golubitsky *et al.* 1988). Consequently, the pattern presented in figure 1*b* should correspond to the cubic symmetry, as, for the given radius of the bubble (2.1 mm) and the driving field frequency (1500 Hz), the mode numbers required for the realization of $\mathbb{I}$ cannot be excited. Note that hexagons observed on the plane surface correspond to the largest subgroup of the circle group $\mathbf{O}(2)$. For $\mathbf{O}(3)$, the subgroups of icosahedral and octahedral symmetry are maximal, thus providing an example of an analogue of the hexagon.

Figure 2 suggests a further advance in pattern classification, specifically by indicating the importance of the 'view from below' which uniquely determines the order of the axis for cyclic and dihedral symmetries. Note that, for high frequencies and intense driving pressures, 'square' patterns on the bubble wall have been observed by Trinh *et al.* (1998).

The influence of surface tension on the growth of instabilities near the threshold has been studied by Birkin *et al.* (2001, 2002, 2004) and Watson *et al.* (2003) for aqueous solutions of potassium ferricyanide and surfactant (Triton X-100) added to the liquid, which significantly modifies the surface tension. For a given bubble, the threshold for Faraday wave generation varies with the amount of surfactant (Triton X-100) added to the liquid. The effective surface tension affects bubble dynamics, not least through controlling the mode number which corresponds to Faraday waves. However, it modifies the ring up time history—the transient process of establishing the steady state—which is governed by the interactions between modes. As the same interactions select the preferred pattern realized on the bubble wall, one can expect that the variation of the surface tension will lead to a change in the observed pattern. This could be used to measure the actual surface tension on the dynamic bubble wall (Watson 2003; Leighton 2007*b*). Such measurements would provide a better value for consideration of, say, the generation of bubbles, droplets and aerosols from the real ocean environment (with its range of contaminants) than would application of an ideal value, or one measured on a flat gas/liquid interface using a Langmuir trough technique (which can differ from the value on the bubble because the dynamic interface can collect and redistribute surface active agents). This difference could have considerable effect on weather and climate and the global distribution of organic materials.

Equation (3.4), though obtained for the bubble parametric instability, has a general form describing bifurcation from spherical symmetry and can arise naturally in a large number of physical (and even biological) applications. The selection of a set of invariants $I_k^4(l)$ and weights Γ_k is dictated by the specific constraints of the problem and in our case is reduced to the set $\{\Gamma_0, I_0^4(l); \Gamma_{n'}, I_{n'}^4(l)\}$. The most evident applications are the formation of 'stardrops' (Brunet & Snoeijer 2011), and the buckling and dynamics of biomedical ultrasonic contrast agents (Versluis *et al.* 2010; Sijl *et al.* 2011). Of course, the breathing mode has no effect on the dynamics of the incompressible drop, which in practice is closely realized by liquid drops in air, where the important role is played by an oscillating substrate or by an acoustic radiation

force (in the case of the levitating drop). However, smaller differences in compressibility occur for drops of one liquid in another, as commonly found in the petrochemical harvesting and transport, pharmaceutical and food production, or in the ocean when petrochemical, chemical or biological agents are dispersed as layers or droplets in the seawater, and here the selection of particle shape can play an important role in the dispersion of one liquid medium in another.

Note that pattern formation on a sphere for the invariants with the lower (cubic) dimension has been analysed earlier (Busse 1975; Sattinger 1980; Matthews 2003). When l is odd, the cubic invariant should be zero (owing to the conservation of parity). For even l, there is a unique invariant that is independent of the specific physical model used. The I^3 set has been used to study convective patterns in a spherical shell, which are relevant to continental drift driven by the fluid motion within the Earth's mantle (Busse 1975), and the growth of tumours, where a growing ball of cells may remain spherical or bifurcate to a non-spherical shape (Chaplain *et al.* 2001). For physical conditions suppressing instability of the even modes, the cubic invariant vanishes and equations (4.3) should be used to describe these phenomena, which illustrates the generality of the model proposed in this paper.

6. Conclusions

To summarize, we have developed an asymptotic weak nonlinear theory (based on the third-order Hamiltonian) for pattern formation on a bubble wall driven near threshold by an acoustic field. The simplest solutions of the derived equations can explain the experimentally observed structures: rolls and squares.

The contribution of A.O.M. was supported by MES SS-3641.2010.5 and RFBR no. 11-05-0212a.

Appendix A. Hamiltonian of a bubble

Consider a gas bubble of radius R_0 in a liquid of density ρ_0 driven by an acoustic wave of 'pump' frequency ω and amplitude of P_m. The first terms of an expansion of the Hamiltonian $H = H_0 + H_1 + H_2 + \cdots$ in powers of canonical variables Π, and ξ have the following analytical representations (Maksimov 2008):

$$\left.\begin{aligned} H_0 &= \frac{1}{2\rho_0 R_0^3}\int \Pi\hat{D}(\Pi)\sin\vartheta\,\mathrm{d}\vartheta\,\mathrm{d}\alpha - \frac{\sigma R_0^2}{2}\int s(\nabla_s^2 s)\sin\vartheta\,\mathrm{d}\vartheta\,\mathrm{d}\alpha \\ &\quad - 4\pi\sigma R_0^2\overline{s^2} + 4\pi P_m R_0^3\bar{s} + 6\pi\gamma\left(P_\infty + \frac{2\sigma}{R_0}\right)R_0^3\overline{s^2} \\ \text{and}\quad H_1 &= \frac{1}{2\rho_0 R_0^3}\int s[(\hat{D}\Pi)^2 - (\nabla_s\Pi)^2 - 4\Pi\hat{D}(\Pi)]\sin\vartheta\,\mathrm{d}\vartheta\,\mathrm{d}\alpha - \frac{8\pi\sigma R_0^2}{3}\overline{s^3} \\ &\quad + 4\pi P_m R_0^3\overline{s^2} + 12\pi\gamma\left(P_\infty + \frac{2\sigma}{R_0}\right)R_0^3\bar{s}\left[\overline{s^2} - \frac{1}{2}(\gamma+1)\bar{s}^2\right], \end{aligned}\right\} \quad \text{(A 1)}$$

where $s \equiv \xi/R_0$, $\bar{A} \equiv (4\pi)^{-1} \int A \sin\vartheta \, \mathrm{d}\vartheta \, \mathrm{d}\alpha$, $\nabla_s \equiv \mathbf{e}_\vartheta \partial/\partial\vartheta + \mathbf{e}_\alpha \sin^{-1}\vartheta \partial/\partial\alpha$ is the surface gradient, $\hat{D} = \left[(1/2) + \sqrt{-\nabla_s^2 + (1/4)}\right]$ is a linear operator and σ is the coefficient of the surface tension. We adopt a polytropic law for the gas bubble with the polytropic exponent γ, where P_∞ is the external pressure in the liquid far from the bubble.

The cubic Hamiltonian H_1 is responsible for the interaction of the monopole and two surface modes (the term H_{mss}),

$$
\begin{aligned}
H_{mss} = \sum_{l=2}^{\infty} \sum_{m=-l}^{l} \frac{\omega_0}{8\sqrt{2\pi}(\rho_0 R_0^3 \omega_0)^{1/2} R_0} \Bigg\{ & (-1)^m (a_{00} a_{lm} a_{l-m} + a_{00}^* a_{lm}^* a_{l-m}^*) \\
& \times \left[3\frac{\omega_l}{\omega_0} + (2l+6) + 2(l+1)\frac{\omega_0}{\omega_l}\left(1 - \frac{\omega_2^2}{6\omega_0^2}\right)\right] + (a_{00} a_{lm} a_{lm}^* + a_{00}^* a_{lm} a_{lm}^*) \\
& \times \left[-6\frac{\omega_l}{\omega_0} + 4(l+1)\frac{\omega_0}{\omega_l}\left(1 - \frac{\omega_2^2}{6\omega_0^2}\right)\right] + (a_{00} a_{lm}^* a_{l-m}^* + a_{00}^* a_{lm} a_{l-m}) \\
& \times \left[3\frac{\omega_l}{\omega_0} - (2l+6) + 2(l+1)\frac{\omega_0}{\omega_l}\left(1 - \frac{\omega_2^2}{6\omega_0^2}\right)\right] \Bigg\}, \qquad \text{(A 2)}
\end{aligned}
$$

and the interaction of the surface modes (the term H_{sss}),

$$
\begin{aligned}
H_{sss} = -\sum_{l_1=2}^{\infty} \sum_{m_1=-l_1}^{l_1} \sum_{l_2=2}^{\infty} \sum_{m_2=-l_2}^{l_2} \sum_{l_3=2}^{\infty} \sum_{m_3=-l_3}^{l_3} & \frac{\overline{Y_{l_1 m_1} Y_{l_2 m_2} Y_{l_2 m_3}}}{4\sqrt{2} R_0} \\
& \times \left(\frac{\omega_{l_2}\omega_{l_3}(l_1+1)}{\rho_0 R_0^3 \omega_{l_1}(l_2+1)(l_3+1)} \right)^{1/2} \Big\{ [(a_{l_1 m_1} a_{l_2 m_2} a_{l_3 m_3} + a_{l_1 -m_1}^* a_{l_2 -m_2}^* a_{l_3 -m_3}^*) \\
& + (-1)^{m_1} (a_{l_1 m_1} a_{l_2 -m_2}^* a_{l_3 -m_3}^* + a_{l_1 -m_1}^* a_{l_2 m_2} a_{l_3 m_3})] \\
& \times \left[(l_2+1)(l_3+1) - \frac{[(l_2+1)l_2 + (l_3+1)l_3]}{2} \right. \\
& \left. + \frac{(l_1+1)l_1}{2} - 2(l_2+1) - 2(l_3+1) + \frac{(l_2+1)(l_3+1)}{18}\frac{\omega_2^2}{\omega_{l_2}\omega_{l_3}} \right] \\
& - [(-1)^{m_2} (a_{l_1 m_1} a_{l_2 -m_2}^* a_{l_3 m_3} + a_{l_1 -m_1}^* a_{l_2 m_2} a_{l_3 -m_3}^*) \\
& + (-1)^{m_3} (a_{l_1 m_1} a_{l_2 m_2} a_{l_3 -m_3}^* + a_{l_1 -m_1}^* a_{l_2 -m_2} a_{l_3 m_3})] \\
& \times \left[(l_2+1)(l_3+1) - \frac{[(l_2+1)l_2 + (l_3+1)l_3]}{2} \right. \\
& \left. + \frac{(l_1+1)l_1}{2} - 2(l_2+1) - 2(l_3+1) - \frac{(l_2+1)(l_3+1)}{18}\frac{\omega_2^2}{\omega_{l_2}\omega_{l_3}} \right] \Big\}. \qquad \text{(A 3)}
\end{aligned}
$$

The average of the spherical harmonics over the sphere can be expressed in terms of the Wigner 3j symbols

$$\overline{Y_{l_1 m_1} Y_{l_2 m_2} Y_{l_3 m_3}} = [(2l_1+1)(2l_2+1)(2l_3+1)(4\pi)^{-1}]^{1/2} \times \begin{pmatrix} l_1 & l_2 & l_3 \\ m_1 & m_2 & m_3 \end{pmatrix} \begin{pmatrix} l_1 & l_2 & l_3 \\ 0 & 0 & 0 \end{pmatrix}. \quad (A\,4)$$

References

Ainslie, M. A. & Leighton, T. G. In press. Review of scattering and extinction cross-sections, damping factors and resonance frequencies of a spherical gas bubble. *J. Acoust. Soc. Am.*

Asaki, T. J. & Marston, P. L. 1997 The effect of a soluble surfactant on quadrupole shape oscillations and dissolution of air bubble in water. *J. Acoust. Soc. Am.* **102**, 3372–3376. (doi:10.1121/1.421007)

Asaki, T. J., Marston, P. L. & Trinh, E. 1993 Shape oscillations of bubbles in water driven by modulated ultrasonic radiation pressure: observation and detection with scattering laser light. *J. Acoust. Soc. Am.* **93**, 706–713. (doi:10.1121/1.405434)

Birkin, P. R., Watson, Y. E. & Leighton, T. G. 2001 Efficient mass transfer from an acoustically oscillated gas bubble. *J. Chem. Soc. Chem. Commun.* **24**, 2650–2651. (doi:10.1039/B107616G)

Birkin, P. R., Watson, Y. E., Leighton, T. G. & Smith, K. L. 2002 Electrochemical detection of Faraday waves on the surface of a gas bubble. *Langmuir* **18**, 2135–2140. (doi:10.1021/la0111001)

Birkin, P. R., Leighton, T. G. & Watson, Y. E. 2004 The use of acoustoelectrochemistry to investigate rectified diffusion. *Ultrason. Sonochem.* **11**, 217–221. (doi:10.1016/j.ultsonch.2004.01.023)

Birkin, P. R., Leighton, T. G. & Vian, C. 2011 *Cleaning apparatus and method, and monitoring thereof.* UK patent application GB2472998 published on 2 March 2011, claiming priority on UK patent application no. 0914836.2 (filed 26 August 2009).

Birkin, P. R., Offin, D. G., Vian, C. J. B., Leighton, T. G. & Maksimov, A. O. In press. Investigation of non-inertial cavitation produced by an ultrasonic horn. *J. Acoust. Soc. Am.*

Blue, J. E. 1967 Resonance of a bubble on an infinite rigid boundary. *J. Acoust. Soc. Am.* **41**, 369–372. (doi:10.1121/1.1910347)

Bremond, N., Arora, M., Ohl, C. D. & Lohse D. 2005*a* Cavitating bubble on patterned surfaces. *Phys. Fluids* **17**, 091111. (doi:10.1063/1.1942514)

Bremond, N., Arora, M., Ohl, C. D. & Lohse, D. 2005*b* Cavitating on surfaces. *J. Phys. Condens. Matter* **17**, S3603–S3608. (doi:10.1088/0953-8984/17/45/054)

Brooks, I. M. *et al.* 2009 Physical exchanges at the air-sea interface: UK–SOLAS Field Measurements. *Bull. Am. Meteorol. Soc.* **90**, 629–644. (doi:10.1175/2008BAMS2578.1)

Brown, T. M. & Kotak, R. 1998 Exoplanets or dynamic atmospheres? The radial velocity and line shape variations of 51 Pegasi and τ Bootis. *Astrophys. J. Suppl. Ser.* **117**, 563–585. (doi:10.1086/313123)

Brunet, P. & Snoeijer, J. H. 2011 Star-drop formed by periodic excitation and on air cushion: a short review. *Eur. Phys. J. Special Topics* **192**, 207–226. (doi:10.1140/epjst/e2011-01375-5)

Busse, F. H. 1975 Patterns of convection in spherical shells. *J. Fluid Mech.* **72**, 67–75. (doi:10.1017/S0022112075002947)

Chaplain, M. A. J., Ganesh, M. & Graham, I. G. 2001 Spatio-temporal pattern formation on spherical surfaces: numerical simulation and application to solid tumor growth. *J. Math. Biol.* **42**, 387–423. (doi:10.1007/s002850000067)

Cross, M. C. & Hohenberg, P. C. 1993 Pattern formation outside of equilibrium. *Rev. Mod. Phys.* **65**, 851–1123. (doi:10.1103/RevModPhys.65.851)

Dangla, R. & Poulain, C. 2010 When sound slows down bubbles. *Phys. Fluids* **22**, 041703. (doi:10.1063/1.3415496)

Doinikov, A. A. 2004 Translational motion of a bubble undergoing shape oscillations. *J. Fluid Mech.* **501**, 1–24. (doi:10.1017/S0022112003006220)

Faraday, M. 1831 On a peculiar class of acoustical figures; and on certain forms assumed by groups of particles upon vibrating elastic surfaces. *Phil. Trans. R. Soc. Lond.* **121**, 299–340. (doi:10.1098/rstl.1831.0018)

Feng, Z. & Leal, L. 1997 Nonlinear bubble dynamics. *Annu. Rev. Fluid Mech.* **29**, 201–247. (doi:10.1146/annurev.fluid.29.1.201)

Gaeta, G. 1985 Gradient property of low order covariants and truncated bifurcation equations for SO(N) symmetries. *Phys. Lett. A* **113**, 114–116. (doi:10.1016/0375-9601(85)90151-3)

Golubitsky, M., Stewart, I. & Schaeffer, D. G. 1988 *Singularities and groups in bifurcation theory*. Berlin, Germany: Springer.

Gorskii, S. M., Zinovev, A. Y. & Chichagov, P. K. 1988 Natural oscillations of a tethered gas bubble in liquids. *Sov. Phys. Acoust.* **34**, 1023–1027.

Howkins, S. D. 1965 Measurements of the resonant frequency of a bubble near a rigid boundary. *J. Acoust. Soc. Am.* **37**, 504–508. (doi:10.1121/1.1909358)

Hullin, C. 1977 Pulsieren de luftblasen in wasser. *Acustica* **37**, 64–72.

Landau, L. D. & Lifshitz E. M. 1977 *Quantum mechanics: non-relativistic theory*. Oxford, UK: Pergamon Press.

Leighton, T. G. 1994 *The acoustic bubble*. New York, NY: Academic Press.

Leighton, T. G. 2004 From seas to surgeries, from babbling brooks to baby scans: the acoustics of gas bubbles in liquids. *Int. J. Mod. Phys. B* **18**, 3267–3314. (doi:10.1142/S0217979204026494)

Leighton, T. G. 2007*a* What is ultrasound? *Prog. Biophys. Mol. Biol.* **93**, 3–83. (doi:10.1016/j.pbiomolbio.2006.07.026)

Leighton, T. G. 2007*b* Preliminary considerations on principles for the determination of difficult bubble parameters *in situ* through Megafrexel high speed photographic observation. ISVR technical report 321, University of Southampton, Southampton, UK.

Leighton, T. G., Lingard, R. J., Walton, A. J. & Field, J. E. 1991 Acoustic bubble sizing by the combination of subharmonic emissions with an imaging frequency. *Ultrasonics* **29**, 319–323. (doi:10.1016/0041-624X(91)90029-8)

Leighton, T. G., Phelps, A. D., Ramble, D. G. & Sharpe, D. A. 1996 Comparison of the abilities of eight acoustic techniques to detect and size a single bubble. *Ultrasonics* **34**, 661–667. (doi:10.1016/0041-624X(96)00053-4)

Leighton, T. G., Ramble D. G. & Phelps, A. D. 1997 The detection of tethered and rising bubbles using multiple acoustic techniques. *J. Acoust. Soc. Am.* **101**, 2626–2635. (doi:10.1121/1.418503)

Longuet-Higgins, M. S. 1989*a* Monopole emission of sound by asymmetric bubble oscillations. 1. Normal modes. *J. Fluid Mech.* **201**, 525–541. (doi:10.1017/S0022112089001035)

Longuet-Higgins, M. S. 1989*b* Monopole emission of sound by asymmetric bubble oscillations. 2. An initial value problem. *J. Fluid Mech.* **201**, 543–565. (doi:10.1017/S0022112089001047)

Longuet-Higgins, M. S. 1992 Nonlinear damping of bubble oscillations by resonant interaction. *J. Acoust. Soc. Am.* **91**, 1414–1422. (doi:10.1121/1.402472)

Maksimov, A. O. 2005 On the volume oscillations of a tethered bubble. *J. Sound Vibration* **283**, 915–926. (doi:10.1016/j.jsv.2004.05.021)

Maksimov, A. O. 2008 Hamiltonian description of bubble dynamics. *J. Exp. Theor. Phys.* **106**, 355–370. (doi:10.1134/S1063776108020143)

Maksimov, A. O. & Leighton, T. G. 2001 Transient processes near the acoustic threshold of parametrically-driven bubble shape oscillations. *Acta Acustica* **87**, 322–332.

Maksimov, A. O., Leighton, T. G. & Birkin, P. R. 2008 Self focusing of acoustically excited Faraday ripples on a bubble wall. *Phys. Lett. A* **372**, 3210–3216. (doi:10.1016/j.physleta.2008.01.041)

Matthews, P. S. 2003 Pattern formation on a sphere. *Phys. Rev. E* **67**, 036206. (doi:10.1103/PhysRevE.67.036206)

Mei, C. C. & Zhou, X. 1991 Parametric resonance of a spherical bubble. *J. Fluid Mech.* **229**, 29–50. (doi:10.1017/S0022112091002926)

Miles, J. 1993 On Faraday waves. *J. Fluid Mech.* **248**, 671–683. (doi:10.1017/S0022112093000965)

Milner, S. T. 1991 Square patterns and secondary instabilities in driven capillary waves. *J. Fluid Mech.* **225**, 81–100. (doi:10.1017/S0022112091001970)

Offin, D. G., Birkin, P. R. & Leighton, T. G. 2007 Electrodeposition of copper in the presence of an acoustically excited gas bubble. *Electrochem. Commun.* **9**, 1062–1068. (doi:10.1016/j.elecom.2006.12.025)

Phelps, A. D. & Leighton, T. G. 1996 High-resolution bubble sizing through detection of the subharmonic response with a two-frequency excitation technique. *J. Acoust. Soc. Am.* **99**, 1985–1992. (doi:10.1121/1.415385)

Prabowo, F. & Ohl, C. D. 2011 Surface oscillation and jetting from surface attached acoustic driven bubbles. *Ultrason. Sonochem.* **18**, 431–435. (doi:10.1016/j.ultsonch.2010.07.013)

Rácz, Z. & Tél, T. 1982 Pattern formation: a Landau-type analysis of symmetry breaking. *Phys. Rev. A* **26**, 2968–2973. (doi:10.1103/PhysRevA.26.2968)

Ramble, D., Phelps, A. & Leighton, T. G. 1998 On the relation between surface waves on a bubble and the subharmonic combination-frequency emission. *Acta Acustica* **84**, 986–988.

Reese, D., Lignières, F. & Rieutord, M. 2006 Acoustic oscillations of rapidly rotating polytropic stars. II. Effects of the Coriolis and centrifugal accelerations. *Astron. Astrophys.* **455**, 621–637. (doi:10.1051/0004-6361:20065269)

Sattinger, D. 1980 Bifurcation and symmetry breaking in applied mathematics. *Bull. Am. Math. Soc.* **3**, 779–819. (doi:10.1090/S0273-0979-1980-14823-5)

Sijl, J. *et al.* 2011 'Compression-only' behavior: a second-order nonlinear response of ultrasound contrast agent microbubbles. *J. Acoust. Soc. Am.* **129**, 1729–1739. (doi:10.1121/1.3505116)

Tho, P., Manasseh, R. & Ooi, A. 2007 Cavitation microstreaming patterns in single and multiple bubble systems. *J. Fluid Mech.* **576**, 191–233. (doi:10.1017/S0022112006004393)

Trinh, E., Thiessen, D. & Holt, R. 1998 Driven and freely decaying nonlinear shape oscillations of drops and bubbles immersed in a liquid: experimental results. *J. Fluid Mech.* **364**, 253–272. (doi:10.1017/S0022112098001153)

Versluis, M., Goertz, D. E., Palanchon, P., Heitman, I. L., van der Meer, S. M., Dollet B., de Jong, N. & Lohse, D. 2010 Microbubble shape oscillations excited through ultrasonic parametric driving. *Phys. Rev. E* **82**, 026321. (doi:10.1103/PhysRevE.82.026321)

Watson, Y. E. 2003 Electrochemical investigations of acoustically driven gas bubbles. PhD thesis, University of Southampton, Southampton, UK.

Watson, Y. E., Birkin, P. R. & Leighton, T. G. 2003 Electrochemical detection of bubble oscillation. *Ultrason. Sonochem.* **10**, 65–69. (doi:10.1016/S1350-4177(02)00149-9)

Weninger, K. R., Cho, R. A., Hiller, R. A., Putterman, S. J. & Williams, G. A. 1997 Sonoluminescence from an isolated bubble on a solid surface. *Phys. Rev. E* **56**, 6745–6749. (doi:10.1103/PhysRevE.56.6745)

Wiggins, S. 1996 *Introduction to applied nonlinear dynamical systems and chaos.* Berlin, Germany: Springer.

Zhang, W. B. & Vinals, J. 1996 Square patterns and quasipatterns in weakly damped Faraday waves. *Phys. Rev. E* **53**, 4283–4286. (doi:10.1103/PhysRevE.53.R4283)